

## Quantum confinement effect in ZnO/Mg<sub>0.2</sub>Zn<sub>0.8</sub>O multishell nanorod heterostructures

Eue-Soon Jang, Jun Young Bae, Jinkyong Yoo, Won Il Park, Dong-Wook Kim, and Gyu-Chul Yi<sup>a)</sup>

National CRI Center for Semiconductor Nanorods and Department of Materials Science and Engineering, Pohang University of Science and Technology (POSTECH), San-31 Hyoja-dong, Pohang, Gyeongbuk 790-784, Korea

T. Yatsui and M. Ohtsu<sup>b)</sup>

Solution-Oriented Research for Science and Technology (SORST), Japan Science and Technology Agency, Machida, Tokyo 194-0004, Japan

(Received 23 May 2005; accepted 15 November 2005; published online 9 January 2006)

We report on photoluminescence measurements of Mg<sub>0.2</sub>Zn<sub>0.8</sub>O/ZnO/Mg<sub>0.2</sub>Zn<sub>0.8</sub>O multishell layers on ZnO core nanorods. Dominant excitonic emissions in the photoluminescence spectra show a blueshift depending on the ZnO shell layer thickness attributed to the quantum confinement effect in the nanorod heterostructure radial direction. Furthermore, near-field scanning optical microscopy clearly shows sharp photoluminescence peaks from the individual nanorod quantum structures, corresponding to subband levels. © 2006 American Institute of Physics. [DOI: 10.1063/1.2162695]

Recent progress in semiconductor nanowire and nanorod heterostructure synthesis allows us to explore high-performance electronic, optoelectronic, and sensing nanodevices.<sup>1–6</sup> Especially, composition-modulated nanowire/nanorod heterostructures have great potential as building blocks for the fabrication of quantum devices, such as high electron mobility transistors.<sup>7</sup> Composition modulation in the radial direction can efficiently confine both the carriers and emitted photons: coaxial nanorod heterostructures are expected to suppress surface state mediated nonradiative recombination and to decrease thermal quenching of emission intensity.<sup>8</sup> Although there have been some reports on coaxial nanowire and nanorod heterostructures, including Ge/Si, Si/CdSe, and GaP/GaN,<sup>9–11</sup> a quantum confinement effect in a multishell nanorod heterostructure has not been reported. The shell layer thicknesses of the reported multishell nanorod heterostructures are a few tens of nm,<sup>3,9,11</sup> which is generally too thick to confine charge carriers in the shell layer.<sup>12,13</sup> Moreover, many of the coaxial nanowire heterostructures show large lattice mismatches between their core and shell layer components (for instance, 11% for Si/CdSe and 71% for GaP/GaN). This will result in strain-induced crystal defects at the interface, which hinders the appearance of quantum confinement.<sup>14</sup> Precise control of shell thickness and a negligible lattice mismatch in ZnO/Mg<sub>0.2</sub>Zn<sub>0.8</sub>O coaxial nanorod heterostructures enable us to successfully demonstrate the quantum confinement effect in multishell quantum structures.

We fabricated ZnO/Mg<sub>0.2</sub>Zn<sub>0.8</sub>O/ZnO/Mg<sub>0.2</sub>Zn<sub>0.8</sub>O multishell nanorod heterostructures on Al<sub>2</sub>O<sub>3</sub>(0001) and Si(100) substrates using catalyst-free metalorganic vapor phase epitaxy (MOVPE). For core ZnO nanorod synthesis, we used diethylzinc and oxygen as the reactants with argon as the carrier gas.<sup>1,14</sup> Subsequent Mg<sub>0.2</sub>Zn<sub>0.8</sub>O shell layers were deposited by introducing bis-cyclopentadienyl-Mg as the Mg precursor. Energy dispersive x-ray spectroscopy

analysis confirmed Mg concentration in the Mg<sub>0.2</sub>Zn<sub>0.8</sub>O layers. The multishell nanorod heterostructures, as schematically depicted in Fig. 1, were prepared by repeated alternate deposition of ZnO and Mg<sub>0.2</sub>Zn<sub>0.8</sub>O layers. The nanorods with various ZnO quantum well (QW) widths,  $L_W$ , were prepared in order to investigate the quantum confinement effect. Such distinctive coaxial nanorod structures were realized by precise control of  $L_W$  and  $L_B$  in angstrom scale using a computer-controlled gas valve system in our MOVPE system. In particular, the formation of interfacial intermediate alloy layers was prevented by purging the system with pure

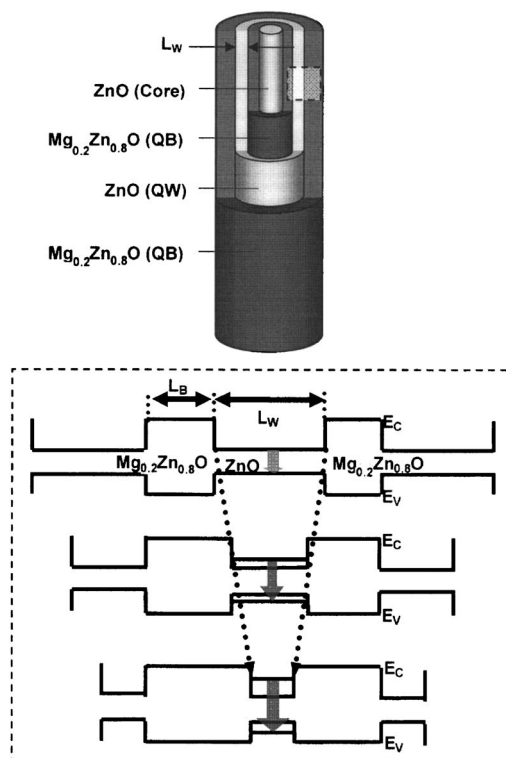


FIG. 1. Schematic illustration of a ZnO/Mg<sub>0.2</sub>Zn<sub>0.8</sub>O/ZnO/Mg<sub>0.2</sub>Zn<sub>0.8</sub>O multishell nanorod heterostructure and its band diagrams for different ZnO (QW) shell widths ( $L_W$ ).

<sup>a)</sup> Author to whom correspondence should be addressed; electronic mail: gcyi@postech.ac.kr

<sup>b)</sup> Also at: the School of Engineering, University of Tokyo, 7-3-1 Hongo, Bunkyo-ku, Tokyo 113-8656, Japan.

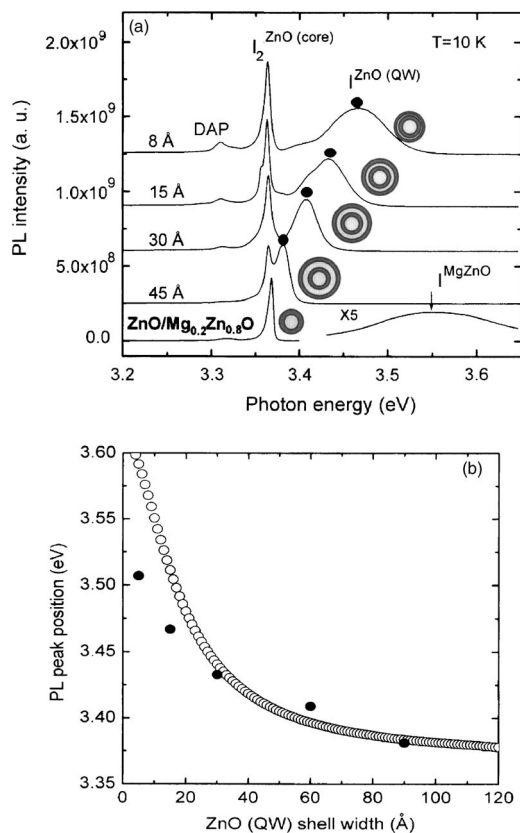


FIG. 2. (a) PL spectra (10 K) of ZnO/Mg<sub>0.2</sub>Zn<sub>0.8</sub>O core/shell nanorod heterostructures and ZnO/Mg<sub>0.2</sub>Zn<sub>0.8</sub>O/ZnO/Mg<sub>0.2</sub>Zn<sub>0.8</sub>O multishell nanorod quantum structures with different ZnO (QW) shell widths of 45, 30, 15, 8 Å. (b) Well-width dependent PL peak positions in ZnO/Mg<sub>0.2</sub>Zn<sub>0.8</sub>O coaxial quantum structures (solid circles) and theoretically calculated values (open circles) in one period of one-dimensional square potential wells. In this calculation, we employed the following parameters: 0.28 and 1.8  $m_0$  for the effective masses of electron and hole, respectively, a ratio of conduction and valence band offsets ( $\Delta E_c/\Delta E_v$ ) of 9, and a band gap offset ( $\Delta E_g$ ) of 250 meV.

argon whenever the reactants were delivered into the system, leading to formation of clean and abrupt interfaces as confirmed by high resolution transmission electron microscopy. A small lattice mismatch (<1%) between ZnO and Mg<sub>0.2</sub>Zn<sub>0.8</sub>O layers is also helpful to reduce defects in the interface.<sup>1,8</sup>

Far-field photoluminescence (PL) measurements were performed using the 325 nm line of a He–Cd laser as an excitation source at 10 K with an optical resolution of 1 Å.<sup>1</sup> To obtain optical spectra from a single nanorod, near-field scanning optical microscopy (NSOM) was used: a sharpened ultraviolet (UV) fiber, coated with a 50-nm-thick aluminum film, was used as a scanning probe, and a He–Cd laser light ( $\lambda=325$  nm) was a light source to excite individual ZnO/Mg<sub>0.2</sub>Zn<sub>0.8</sub>O/ZnO/Mg<sub>0.2</sub>Zn<sub>0.8</sub>O multishell nanorods through the UV fiber probe.<sup>15</sup> The fiber probe was used not only for excitation but also for collecting PL signals from the nanorods. The fiber probe was kept in close proximity to the sample surface ( $\sim 10$  nm) using the shear-force feedback technique. The probe collected light signal was analyzed by a monochromator and the intensity was measured by a cooled charge coupled device.

The general morphology of the nanorod heterostructures was investigated using field-emission scanning electron microscopy. The mean diameter and length of bare ZnO nanorods, grown at 800 °C for 2 h, are 26 nm and 2.5  $\mu$ m, re-

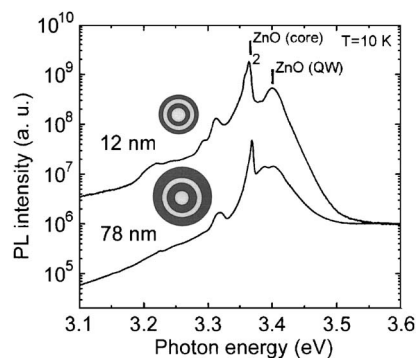


FIG. 3. PL spectra (10 K) of ZnO/Mg<sub>0.2</sub>Zn<sub>0.8</sub>O/ZnO/Mg<sub>0.2</sub>Zn<sub>0.8</sub>O multishell nanorods upon variation of different Mg<sub>0.2</sub>Zn<sub>0.8</sub>O (QB) shell widths of 12 and 78 nm. The Mg<sub>0.2</sub>Zn<sub>0.8</sub>O (QB) shell layer thickness was fixed at 120 Å. Cross-sectional views, ZnO (QW) shell widths, and Mg<sub>0.2</sub>Zn<sub>0.8</sub>O (QB) barrier widths of coaxial nanorod heterostructures are depicted in the inset, respectively.

spectively. Subsequent growth processes of the ZnO (QW) and Mg<sub>0.2</sub>Zn<sub>0.8</sub>O (QB) shell layers gradually increased the nanorod diameter: a growth time of QB layer of 30, 60, and 180 s produced nanorod heterostructures with various diameters of 51, 52, and 58 nm, respectively. Growth rates of the ZnO (QW) and Mg<sub>0.2</sub>Zn<sub>0.8</sub>O (QB) shells were roughly 0.25 and 0.33 Å/s.

Figure 2(a) shows 10 K PL spectra of the ZnO/Mg<sub>0.2</sub>Zn<sub>0.8</sub>O core/shell and ZnO/Mg<sub>0.2</sub>Zn<sub>0.8</sub>O/ZnO/Mg<sub>0.2</sub>Zn<sub>0.8</sub>O multishell nanorod heterostructures. The schematic diagrams of the heterostructures are also shown in Fig. 2(a). PL spectra of the ZnO/Mg<sub>0.2</sub>Zn<sub>0.8</sub>O core/shell nanorods exhibited two dominant PL peaks at 3.364 and 3.553 eV corresponding to excitonic emissions from ZnO core nanorods ( $I_2^{\text{ZnO(core)}}$ ) and Mg<sub>0.2</sub>Zn<sub>0.8</sub>O ( $I^{\text{MgZnO}}$ ) shell layers, respectively.<sup>1,16–18</sup> Except for these PL peaks, no PL peak is shown in the range between 3.364 and 3.553 eV, strongly suggesting that there is no significant intermediate layer formation between ZnO core and Mg<sub>0.2</sub>Zn<sub>0.8</sub>O shell layers. If there is an intermediate layer between the ZnO core and Mg<sub>0.2</sub>Zn<sub>0.8</sub>O shell layers, there should be at least one additional PL peak between 3.364 and 3.553 eV.

Meanwhile, ZnO/Mg<sub>0.2</sub>Zn<sub>0.8</sub>O/ZnO/Mg<sub>0.2</sub>Zn<sub>0.8</sub>O core/multishell nanorod heterostructures with various  $L_W$ , from 8 to 45 Å, and fixed  $L_B$  of 120 Å, showed a new PL peak marked by  $I^{\text{ZnO(QW)}}$ . The  $I^{\text{ZnO(QW)}}$  peak energy increases from 3.382 to 3.467 eV, as the  $L_W$  is decreased from 45 to 8 Å. All the  $I^{\text{ZnO(QW)}}$  peaks blueshift toward higher energy, compared with 3.364 eV of  $I^{\text{ZnO(core)}}$ . Such a blueshift of the PL emission peak can be well understood by the fact that quantized sublevel states are created due to the quantum size effect in core/multishell nanorod heterostructures and quantized energy levels increase by decreasing the embedded ZnO (QW) shell layer width,  $L_W$ .<sup>19,20</sup> Figure 2(b) also shows the dominant PL peak positions obtained from experiments and theoretical predictions in finite periodic square-well potential of ZnO/Mg<sub>0.2</sub>Zn<sub>0.8</sub>O/ZnO/Mg<sub>0.2</sub>Zn<sub>0.8</sub>O core/multishell nanorods. As shown in Fig. 2(b), the experimental values agree well with the theoretical calculation except small deviation for the samples with the narrow quantum well widths below 20 Å, indicating that the systematic increase in PL emission energy with reducing well width is consistent with the quantum confinement effect.

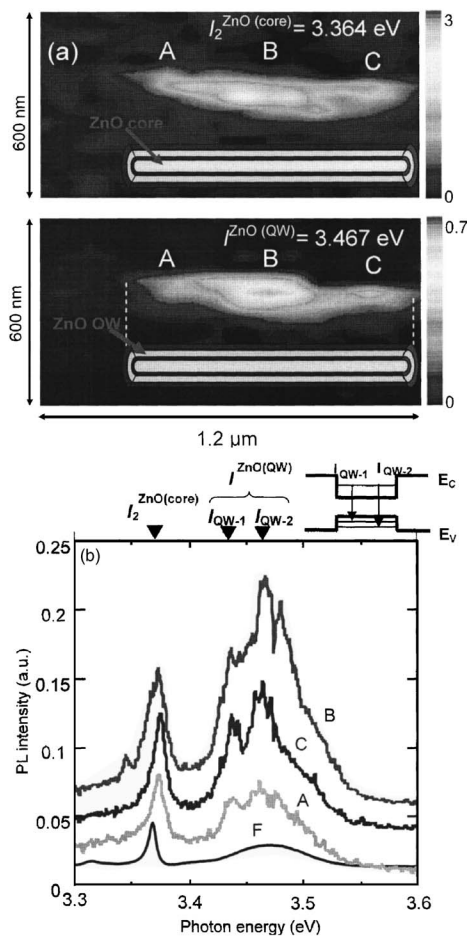


FIG. 4. (a) Monochromatic PL images of  $\text{ZnO}/\text{Mg}_{0.2}\text{Zn}_{0.8}\text{O}/\text{ZnO}/\text{Mg}_{0.2}\text{Zn}_{0.8}\text{O}$  multishell nanorods measured at different emission energies of 3.364 ( $I_2^{\text{ZnO}(\text{core})}$ ) and 3.467 ( $I_2^{\text{ZnO}(\text{QW})}$ ) eV. In the  $\text{ZnO}/\text{Mg}_{0.2}\text{Zn}_{0.8}\text{O}$  core/multishell nanorod quantum structures, ZnO (QW) and  $\text{Mg}_{0.2}\text{Zn}_{0.8}\text{O}$  shell widths are 8 and 120 Å, respectively. (b) Near-field PL spectra taken at different positions marked by A, B, and C in (a). The black solid curve (F) is the far-field spectrum.

Compositional intermixing of ZnO and  $\text{Mg}_{0.2}\text{Zn}_{0.8}\text{O}$  at the interface also may cause a blueshift of the PL peaks. To rule out this possibility, we prepared  $\text{ZnO}/\text{Mg}_{0.2}\text{Zn}_{0.8}\text{O}/\text{ZnO}/\text{Mg}_{0.2}\text{Zn}_{0.8}\text{O}$  multishell nanorods with two different  $L_W$  (12 and 78 nm) and fixed  $L_B$  (30 Å). Intermixing at the interface may cause a couple of effects: (1) the Mg mole fraction in the alloy becomes higher by increasing the  $\text{Mg}_{0.2}\text{Zn}_{0.8}\text{O}$  shell layer thickness (or growth time), resulting in a larger PL peak blueshift;<sup>21</sup> (2) effective ZnO (QW) shell thickness can be altered. As shown in Fig. 3, the  $I_2^{\text{ZnO}(\text{QW})}$  peak positions of the two nanorods are nearly the same, ruling out the intermixing possibility.

Furthermore, we examined spatially resolved PL properties of a single nanorod quantum structure by near-field scanning optical microscopy (NSOM). Figures 4(a) and 4(b) show the near-field images and spectra of a  $\text{ZnO}/\text{Mg}_{0.2}\text{Zn}_{0.8}\text{O}/\text{ZnO}/\text{Mg}_{0.2}\text{Zn}_{0.8}\text{O}$  multishell nanorod with  $L_W$  of 8 Å and  $L_B$  of 120 Å. As shown in Fig. 4(a), near-field PL intensity distribution taken at two photon energies of 3.364 (corresponding to  $I_2^{\text{ZnO}(\text{core})}$ ) and 3.467 eV (corresponding to  $I_2^{\text{ZnO}(\text{QW})}$ ) are very similar, except for topographically induced emission intensity variation. This indicates that uniform ZnO core and shell layers form along the axial direction of the multishell nanorod. In addition, near-field PL spectra, collected from different positions as

denoted by A, B and C in Fig. 4(a), were obtained as shown in Fig. 4(b). This result demonstrates that constituent layers of the multishell nanorod, ZnO and  $\text{Mg}_{0.2}\text{Zn}_{0.8}\text{O}$ , are homogeneously grown throughout the entire nanorod heterostructures.

It is worth noting that near-field PL spectra show two distinct peaks at 3.435 ( $I_{\text{QW}-1}$ ) and 3.460 ( $I_{\text{QW}-2}$ ) eV [Fig. 4(b)] [far-field PL spectra exhibited only a single peak at 3.467 eV [Fig. 2(a)]. The  $I_{\text{QW}-1}$  and  $I_{\text{QW}-2}$  are PL emission peaks due to the ground state of the electrons and the two different valence band states of the holes as depicted in the upper right side of Fig. 4(b).

In conclusion, catalyst-free MOVPE demonstrates fabrication of high quality  $\text{ZnO}/\text{Mg}_{0.2}\text{Zn}_{0.8}\text{O}/\text{ZnO}/\text{Mg}_{0.2}\text{Zn}_{0.8}\text{O}$  multishell nanorod quantum structures by fine tuning the ZnO (QW) and  $\text{Mg}_{0.2}\text{Zn}_{0.8}\text{O}$  (QB) shell thicknesses. From both far-field and near-field PL spectra of the nanorod quantum structures, systematic PL blueshifts with decreasing well layer widths were observed, resulting from the quantum confinement effect. This controlled growth of coaxial multishell nanorod quantum structures realizes the artificial design of a kind of semiconductor nanorod quantum structures, which could open up significant opportunities for exploring high performance electronic and photonic nanodevices.

This work was financially supported through the National Creative Research Initiative Project by the KOSEF and the Air Force Office of Scientific Research (FA5209-04-P-0325), USA.

<sup>1</sup>W. I. Park, G.-C. Yi, M. Kim, and S. J. Pennycook Adv. Mater. (Weinheim, Ger.) **15**, 526 (2003).

<sup>2</sup>S. W. Jung, W. I. Park, G.-C. Yi, and M. Kim, Adv. Mater. (Weinheim, Ger.) **15**, 1358 (2003).

<sup>3</sup>J. Hu, Y. Bando, Z. Liu, T. Sekiguchi, D. Goldberg, and J. Zhan, J. Am. Chem. Soc. **125**, 11306 (2003).

<sup>4</sup>D. Li, Y. Wu, R. Fan, P. Yang, and A. Majumdar, Appl. Phys. Lett. **83**, 3186 (2003).

<sup>5</sup>X. Wang, C. J. Summers, and Z. L. Wang, Adv. Mater. (Weinheim, Ger.) **16**, 1215 (2004).

<sup>6</sup>C. Thelander, T. Mårtensson, M. T. Björk, B. J. Ohlsson, M. W. Larsson, L. R. Wallenberg, and L. Samuelson, Appl. Phys. Lett. **83**, 2052 (2003).

<sup>7</sup>Y. Wu, J. Xiang, C. Yang, W. Lu, and C. M. Lieber, Nature (London) **430**, 61 (2004).

<sup>8</sup>W. I. Park, S. J. An, G.-C. Yi, and M. Kim, *Fourth IEEE Conference Proceeding on Nanotechnology* (IEEE, New York, 2004), p. 83.

<sup>9</sup>L. J. Lauhon, M. S. Gudiksen, D. Wang, and C. M. Lieber, Nature (London) **57**, 420 (2002).

<sup>10</sup>Q. Li and C. Wang, J. Am. Chem. Soc. **125**, 9892 (2003).

<sup>11</sup>H.-M. Lin, Y.-L. Chen, J. Yang, Y.-C. Liu, K.-M. Yin, J. J. Kai, F.-R. Chen, L.-C. Chen, Y.-F. Chen, and C.-C. Chen, Nano Lett. **3**, 537 (2003).

<sup>12</sup>K. K. Nanda, F. E. Kruijs, and H. Fissan, Nano Lett. **1**, 605 (2001).

<sup>13</sup>H. Yu, J. Li, R. A. Loomis, L.-W. Wang, and W. E. Buhro, Nat. Mater. **2**, 517 (2003).

<sup>14</sup>S. J. An, W. I. Park, G.-C. Yi, Y.-J. Kim, H.-B. Kang, and M. Kim, Appl. Phys. Lett. **84**, 3612 (2004).

<sup>15</sup>W. I. Park, S. J. An, J. L. Yang, G.-C. Yi, S. Hong, T. Joo, and M. Kim, J. Phys. Chem. B **108**, 15457 (2004).

<sup>16</sup>T. Yatsui, J. Lim, M. Ohtsu, S. J. An, and G.-C. Yi, Appl. Phys. Lett. **85**, 727 (2004).

<sup>17</sup>S. Fujita, T. Takagi, H. Tanaka, and S. Fujita, Phys. Status Solidi B **241**, 599 (2004).

<sup>18</sup>H. Kato, M. Sano, K. Miyamoto, and T. Yao, Phys. Status Solidi B **241**, 612 (2004).

<sup>19</sup>A. Ohtomo, K. Tamura, I. Ohkubo, H. Koinuma, T. Yasuda, and Y. Segawa, Appl. Phys. Lett. **75**, 980 (1999).

<sup>20</sup>T. Makino, C. H. Chia, Ng. T. Tuan, H. D. Sun, Y. Segawa, M. Kawasaki, A. Ohtomo, K. Tamura, and H. Koinuma, Appl. Phys. Lett. **77**, 975 (2000).

<sup>21</sup>W. I. Park, G.-C. Yi, and H. M. Jang, Appl. Phys. Lett. **79**, 2022 (2001).